Full-field time-encoded frequency-domain optical coherence tomography

Boris Považay, Angelika Unterhuber, Boris Hermann, Harald Sattmann

Center of Biomedical Engineering and Physics, Christian Doppler Laboratory, Medical University Vienna, A-1090 Vienna, Austria

Holger Arthaber

Institute of Electrical Measurements and Circuit Design, Vienna University of Technology, A-1040 Vienna, Austria

Wolfgang Drexler

Center of Biomedical Engineering and Physics, Christian Doppler Laboratory, Medical University Vienna, A-1090 Vienna, Austria
wolfgang.drexler@meduniwien.ac.at

Abstract: Ultrahigh axial resolution surface profiling as well as volumetric optical imaging based on time encoded optical coherence tomography in the frequency domain without any mechanical scanning element is presented. A frequency tuned broad bandwidth titanium sapphire laser is interfaced to an optical microscope (Axioskop 2 MAT, Carl Zeiss Meditec) that is enhanced with an interferometric imaging head. The system is equipped with a 640 x 480 pixel CMOS camera, optimized for the 800 nm wavelength tuning range for transmission and reflection measurements of a microscopic sample. Sample volume information over 1.3 x 1 x 0.2 mm³ with ~3 µm axial and ~4 µm transverse resolution in tissue is acquired by a single wavelength scan over more than 100 nm optical bandwidth from <760 to >860 nm with 128-2048 equidistant optical frequency steps with an acquisition time of 1 to 50 ms per step. Topography and tomography with a signal to noise ratio of 83 dB is demonstrated on test surfaces and biological specimen respectively. This novel OCT technique promises to enable high speed, three dimensional imaging by employing high frame rate cameras and state of the art tunable lasers in a mechanically stable environment, due to lack of moving components while reducing the intensity on the sample.

OCIS codes: (170.4500) optical coherence tomography; (140.3600) Lasers, tunable; (070.2590) Fourier transforms; (180.6900) Three-dimensional microscopy; (170.6960) Tomography; (140.3590) Lasers, titanium; (140.3580) Lasers, solid-state; (140.3070) Infrared and far-infrared lasers; (110.6880) Three-dimensional image acquisition

References and links

1. D. Huang, E. A. Swanson, C. P. Lin, J. S. Schuman, W. G. Stinson, W. Chang, M. R. Hee, T. Flotte, K. Gregory, C. A. Puliafito, and J. G. Fujimoto, "Optical Coherence Tomography," Science **254**, 1178-1181 (1991).
2. E. A. Swanson, D. Huang, M. R. Hee, J. G. Fujimoto, C. P. Lin, and C. A. Puliafito, "High-speed optical coherence domain reflectometry," Opt. Lett. **17**, 151-153 (1992).
3. W. Drexler, U. Morgner, F. X. Kartner, C. Pitris, S. A. Boppart, X. D. Li, E. P. Ippen, and J. G. Fujimoto, "In vivo ultrahigh-resolution optical coherence tomography," Opt. Lett. **24**, 1221-1223 (1999).
4. W. Drexler, U. Morgner, R. K. Ghanta, F. X. Kartner, J. S. Schuman, and J. G. Fujimoto, "Ultrahigh-resolution ophthalmic optical coherence tomography," Nat. Med. **7**, 502-507 (2001).
5. W. Drexler, "Ultrahigh-resolution optical coherence tomography," J. Biomed. Opt. **9**, 47-74 (2004).
6. B. Považay, K. Bizheva, A. Unterhuber, B. Hermann, H. Sattmann, A. F. Fercher, W. Drexler, A. Apolonski, W. J. Wadsworth, J. C. Knight, P. S. J. Russell, M. Vetterlein, and E. Scherzer, "Submicrometer axial resolution optical coherence tomography," Opt. Lett. **27**, 1800-1802 (2002).
7. A. M. Rollins, M. D. Kulkarni, S. Yazdanfar, R. Ung-arunyawee, and J. A. Izatt, "In vivo video rate optical coherence tomography," Opt. Express **3**, 219-229 (1998).
8. C. Hauger, M. Worz, and T. Hellmuth, "Interferometer for optical coherence tomography," Appl. Opt. **42**, 3896-

#69358 - $15.00 USD Received 27 March 2006; revised 19 June 2006; accepted 20 June 2006

3902 (2003).
9. A. Dubois, K. Grieve, G. Moneron, R. Lecaque, L. Vabre, and C. Boccara, "Ultrahigh-resolution full-field optical coherence tomography," Appl. Opt. **43**, 2874-2883 (2004).
10. Y. Yasuno, Y. Sutoh, M. Nakama, S. Makita, M. Roh, T. Yatagai, and M. Mori, "Spectral interferometric optical coherence tomography with nonlinear beta-barium borate time gating," Opt. Lett. **27**, 403-405 (2002).
11. "Spectroscopic techniques for far infra-red, submillimetre and millimetre waves," D. H. Martin, ed. (North-Holland Publishing Co, Amsterdam, Netherlands, 1967), p. 400.
12. S. H. Yun, G. J. Tearney, J. F. de-Boer, N. Iftimia, and B. E. Bouma, "High-speed optical frequency-domain imaging," Opt. Express **11** (2003).
13. A. F. Fercher, C. K. Hitzenberger, G. Kamp, and S. Y. El-Zaiat, "Measurement of intraocular distances by back-scattering spectral interferometry," Opt. Commun. **117**, 43-48 (1995).
14. B. Golubovic, B. E. Bouma, G. J. Tearney, and J. G. Fujimoto, "Optical frequency-domain reflectometry using rapid wavelength tuning of a Cr^{4+}:forsterite laser," Opt. Lett. **22**, 1704-1706 (1997).
15. F. Lexer, C. K. Hitzenberger, A. F. Fercher, and M. Kulhavy, "Wavelength-tuning interferometry of intraocular distances," Appl. Opt. **36**, 6548-6562 (1997).
16. G. Hausler, and M. W. Linduer, ""Coherence radar" and "spectral radar"-new tools for dermatological diagnosis," J. Biomed. Opt. **3**, 21-31 (1998).
17. R. Leitgeb, C. K. Hitzenberger, and A. F. Fercher, "Performance of fourier domain vs. time domain optical coherence tomography," Opt. Express **11**, 889-894 (2003).
18. M. A. Choma, M. V. Sarunic, C. H. Yang, and J. A. Izatt, "Sensitivity advantage of swept source and Fourier domain optical coherence tomography," Opt. Express **11**, 2183-2189 (2003).
19. J. F. de Boer, B. Cense, B. H. Park, M. C. Pierce, G. J. Tearney, and B. E. Bouma, "Improved signal-to-noise ratio in spectral-domain compared with time-domain optical coherence tomography," Opt. Lett. **28**, 2067-2069 (2003).
20. M. Wojtkowski, R. Leitgeb, A. Kowalczyk, T. Bajraszewski, and A. F. Fercher, "In vivo human retinal imaging by Fourier domain optical coherence tomography," J. Biomed. Opt. **7**, 457-463 (2002).
21. W. Y. Oh, S. H. Yun, G. J. Tearney, and B. E. Bouma, "115 kHz tuning repetition rate ultrahigh-speed wavelength-swept semiconductor laser," Opt. Lett. **30**, 3159-3161 (2005).
22. R. A. Leitgeb, W. Drexler, A. Unterhuber, B. Hermann, T. Bajraszewski, T. Le, A. Stingl, and A. F. Fercher, "Ultrahigh resolution Fourier domain optical coherence tomography," Opt. Express **12**, 2156-2165 (2004).
23. M. Wojtkowski, V. J. Srinivasan, T. H. Ko, J. G. Fujimoto, A. Kowalczyk, and J. S. Duker, "Ultrahigh-resolution, high-speed, Fourier domain optical coherence tomography and methods for dispersion compensation," Opt. Express **12**, 2404-2422 (2004).
24. B. Cense, and N. A. Nassif, "Ultrahigh-resolution high-speed retinal imaging using spectral-domain optical coherence tomography," Opt. Express **12**, 2435-2447 (2004).
25. R. A. Leitgeb, L. Schmetterer, W. Drexler, A. F. Fercher, R. J. Zawadzki, and T. Bajraszewski, "Real-time assessment of retinal blood flow with ultrafast acquisition by color Doppler Fourier domain optical coherence tomography," Opt. Express **11**, 3116-3121 (2003).
26. B. R. White, M. C. Pierce, N. Nassif, B. Cense, B. Hyle Park, G. J. Tearney, B. E. Bouma, T. C. Chen, and J. F. de Boer, "In vivo dynamic human retinal blood flow imaging using ultra-high-speed spectral domain optical coherence tomography," Opt. Express **11**, 3490 (2003).
27. N. A. Nassif, B. Cense, B. H. Park, M. C. Pierce, S. H. Yun, B. E. Bouma, G. J. Tearney, T. C. Chen, and J. F. de Boer, "In vivo high-resolution video-rate spectral-domain optical coherence tomography of the human retina and optic nerve," Opt. Express **12**, 367-376 (2004).
28. M. Wojtkowski, A. Kowalczyk, R. Leitgeb, and A. F. Fercher, "Full range complex spectral optical coherence tomography technique in eye imaging," Opt. Lett. **27**, 1415-1417 (2002).
29. A. Dubois, G. Moneron, K. Grieve, and A. C. Boccara, "Three-dimensional cellular-level imaging using full-field optical coherence tomography," Phys. Med. Biol. **49**, 1227-1234 (2004).
30. G. Moneron, A. C. Boccara, and A. Dubois, "Stroboscopic ultrahigh-resolution full-field optical coherence tomography," Opt. Lett. **30**, 1351-1353 (2005).
31. B. Grajciar, M. Pircher, A. F. Fercher, and R. A. Leitgeb, "Parallel Fourier domain optical coherence tomography for in vivo measurement of the human eye," Opt. Express **13**, 1131-1137 (2005).
32. T. Endo, Y. Yasuno, F. Truffer, G. Aoki, S. Makita, M. Itoh, and T. Yatagai, "Line-field Fourier-domain optical coherence tomography," Proceedings of the SPIE The International Society for Optical Engineering **5690**, 168-173 (2005).
33. L. F. Yu, and M. K. Kim, "Full-color three-dimensional microscopy by wide-field optical coherence tomography," Opt. Express **12**, 6632-6641 (2004).
34. D. Yelin, B. E. Bouma, N. Iftimia, and G. J. Tearney, "Three-dimensional spectrally encoded imaging," Opt. Lett. **28**, 2321-2323 (2003).
35. A. Unterhuber, B. Považay, K. Bizheva, B. Hermann, H. Sattmann, A. Stingl, T. Le, M. Seefeld, R. Menzel, M. Preusser, H. Budka, C. Schubert, H. Reitsamer, P. K. Ahnelt, J. E. Morgan, A. Cowey, and W. Drexler, "Advances in broad bandwidth light sources for ultrahigh resolution optical coherence tomography," Phys. Med. Biol. **49**, 1235-1246 (2004).
36. M.-K. Kim, "Tomographic three-dimensional imaging of a biological specimen using wavelength-scanning digital interference holography," Opt. Express **7**, 305 (2000).

#69358 - $15.00 USD Received 27 March 2006; revised 19 June 2006; accepted 20 June 2006

1. Introduction

Optical coherence tomography (OCT) is a non-invasive, cross-sectional imaging technique that measures depth resolved reflectance of tissue by employing low-coherence interferometry [1]. The acquisition of the signal may be achieved either in the time domain (TD) by altering the reference arm length of the interferometer, or in the frequency domain (FD) where the individual spectral frequency components of the interference signal are acquired. To successfully apply OCT as a diagnostic imaging modality performing optical biopsy, i.e. visualization of tissue morphology at resolutions approaching the level of histopathology, in the range of less than 3 µm in tissue in addition to a short measuring time for the whole investigated volume is necessary to reduce motion artifacts. Imaging sensitivity is directly connected to the number of photons or energy per area element. However, exposure of living biological tissue is primarily limited by maximum local optical power on the sample, rather than dosage. This leaves no way to improve imaging speed of huge numbers of voxels with single beam scanning systems, even when high power sources become available. In contrast to lateral resolution, the axial resolution of an OCT system is not only determined by the central wavelength of the light applied, but is also inversely proportional to its bandwidth [2]. Ultrahigh resolution optical coherence tomography (UHR OCT) [3-5] has been established employing state of the art broad bandwidth light source technology enabling *in vivo* visualization of microscopic features of tissue down to the cellular level [6]. These first ultrahigh resolution OCT systems performed visualization of tissue microstructure in the so-called time domain. In this case depth information is obtained as a function of axial reference mirror translation. Depth scanning delay lines providing high scanning speeds of up to 4 kHz, that means 4000 A-scans or lines per second have been developed [7] with the drawback of lower system sensitivity at higher scanning speed and shorter scanning range. Single beam scanning TD-OCT systems filter only one voxel (volume element) at a time, although the full beam power hits the sample. Simultaneous TD depth-extraction [8] (fig.1 bottom left) or parallel imaging techniques [9] (Fig. 1 top left) suffer from this filtering problem, where most of the signal's information is lost in the background. Alternative techniques adopting optically nonlinear filtering mechanism [10] are highly complicated and hardly compatible with the low intensities that are inherent to biomedical imaging systems.

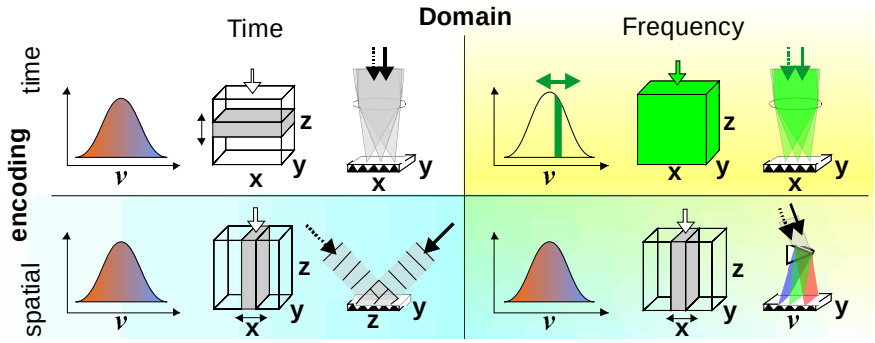

Fig. 1. Comparison of "full field"-OCT technologies, customizing 2D-arrays for acquisition of a 3D-volume. Inlets from left to right depict used frequency range, sample volume where information is extracted from (z=depth=illumination from the top) and detection scheme with the reference beam indicated by a dashed arrow and the sample light by a solid one; detection parameters are marked. Double headed arrows indicate scanning in spatial direction or in frequency. Top left – **teTD** (time encoded time domain) "parallel en face" imaging; bottom left – **seTD** (spatially encoded time domain) parallel imaging in the time domain based on linear superposition of the sample and reference fields, depth is encoded by spatial distribution of different delays (this method has only been demonstrated with a linear array); bottom right – **seFD** (spatially encoded frequency domain) operating like a parallel set of spectrometers; top right – **teFD** (time encoded frequency domain), acquisition of the full volume, successively at different optical frequencies.

#69358 - $15.00 USD Received 27 March 2006; revised 19 June 2006; accepted 20 June 2006

2. Time domain versus frequency domain technologies

The basic phenomena and relationship between time and frequency domain have already been exploited in detail half a century ago [11] when detector technology was restricting access to wide ranges of the electromagnetic spectrum. Therefore an alternative operating by Fourier transformation of the interferometric time domain signal, namely "Fourier transform spectroscopy" or later on "time domain spectroscopy" was established. To distinguish in a structured way between the alternative OCT technologies we will follow the naming convention strictly based on the physical principle, rather than deriving the names from the specific technical apparatus. These involve time and frequency, the information encoding principle as well as the number of dimensions the acquisition system can discriminate without translational scanning of the probing beam. In frequency domain OCT the optical frequency components are captured either time encoded (te) in sequence [12-16] ("swept source OCT", "spectral domain OCT") or simultaneously by spatial encoding (se) with a dispersive element [17-19] ("Fourier domain", "Fourier transform", "spectral domain" OCT). In contrast to time domain acquisition in the FD-technique the spatial frequency information of the whole A-scan (depth scan) is saved in every frequency slot and positional information is not lost. The associated gain in signal to noise ratio is mainly proportional to the number of simultaneously illuminated pixels but might be reduced by the lower dynamics of detector arrays when an integrating CCD detector array is used [17, 19]. Hence both, teFD (Fig. 1 top right) and seFD approach (Fig. 1 bottom right) give access to a higher SNR or acquisition speed at constant illumination power. Due to decoupling of the scanning range and electronic detection bandwidth, FD-OCT enables a significant sensitivity advantage that allows a dramatically increase in line rate (A-scan rate) without loosing imaging performance in comparison to time domain OCT. Frequency domain OCT has recently been demonstrated to enable high speed scanning [20, 21], ultrahigh resolution [22-24] functional imaging [25, 26] and even allows for low speed 3D tissue visualization [27] by fast transversal scanning the imaging beam.

In one-dimensional (1D) point by point raster scanning systems the spectrometer based seFD-OCT is inherently superior to teFD-OCT in terms of phase stability (insensitive to "phase wash-out") due to simultaneous exposure of all frequency slots, though it can be compensated by high speed wavelength swept light sources and the higher dynamic range of single point detectors, especially when used in dual balanced geometry.

However, FD-OCT technology has also remarkable drawbacks. Simple detection in the frequency domain usually lacks of the imaginary signal component, resulting in phenomena like mirroring at the zero-delay due to spatial frequency ambiguity, autocorrelation artifacts, originating from internal interferences of the sample and the system, as well as depth dependent SNR loss, caused by finite spectral line width. Furthermore non-uniform FD sampling deteriorates TD signal quality and time consuming post-processing is a necessity for all FD-OCT techniques. It was found that some of these effects can be largely compensated by multiple, phase shifted imaging of the same region (i.e. A-scan), followed by reconstruction of the complex phase of the FD-signal [28], re-sampling and definite transformation to the time domain.

3. Parallel acquisition techniques

Imaging speed of biological tissue with 1D-FD-OCT at high SNR lies in the 20-40 Mvoxel/s range, which is already much better than the 10-40 kvoxel/s of 1D-teTD-OCT, but is far behind the goal of distortion free 3D imaging at the 4-8 Gvoxel/s range to extract volumes of ~512 x 512 x 512 voxels at 25-60 Hz (=video rate) due to power limitations. Another major disadvantage in 1D scanning systems is the mechanical scanner pair that gives rise to motion artifacts due to mechanical jitter and limited repeatability. These effects adversely deteriorate imaging quality, especially at high imaging speeds and at high resolutions for cellular level tomography. To improve imaging speed, transversally multi-dimensional techniques have already been extensively investigated for TD-OCT imaging in detail [9, 29, 30], which profit of continued high speed camera development with full frame acquisition in the multi kframe/s

#69358 - $15.00 USD Received 27 March 2006; revised 19 June 2006; accepted 20 June 2006

range as well as of the high stability due to the transversally static setup. Their major advantage is found in almost isotropic high resolution sampling of microscopic specimen (within the depth of field), but suffers from low imaging speed and high power requirements because of very low signal to noise, limiting *in vivo* applications. Parallel 2D-seFD-OCT techniques (i.e. ”Line-Field FD-OCT”) based on the introduction of one transversal imaging dimension and detection by a highly parallel spectrometer have been investigated by multiple groups [31, 32]. These seem to have potential for high speed acquisition of cross-sectional scans, but involve a complicated mixture of geometrical imaging in one sensor axis and a spectrometer setup in the orthogonal direction, that confines area detectors to rather low pixel counts due to crosstalk in the “spatial” axis. For full volume acquisition they still need beam translation. To overcome the limitations of the spectrometer based approaches mentioned above, we try to demonstrate a highly parallel extension of time encoded frequency domain OCT, where the spectrum is equidistantly stepped through while full 2D images of the sample are taken for every successive optical frequency step within the specified range. The advantages of this method are its intrinsically high speed and mechanical stability due to the lack of mechanical components, combined with a simple setup, while low scanning rates of the source in the range of 25-60 sweeps per second already would allow for three dimensional OCT imaging with video rate. In contrast to the technique of phase-shift interference [33] or spectrally encoded [34] imaging no moving element is used at all. The setup is based on proven technologies, like standard high quality optics, progress in fast high resolution cameras and swept lasers favors continuous improvements. Since the whole volume information of the investigated sample, limited by the depth of field, is obtained by a single tuning of the laser and no transversal scanning is involved, according to the systematic naming convention introduced above the technique may be called three dimensional, time encoded Frequency domain Optical Coherence Tomography (3D-teFD OCT).

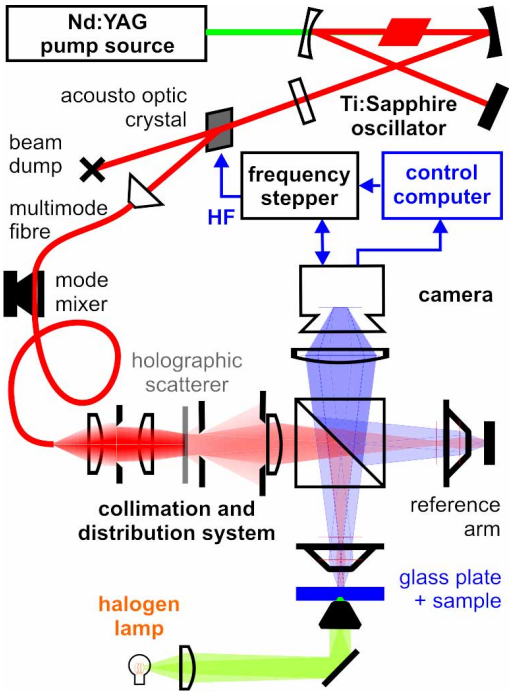

Fig. 2. Schematics of the set-up: Broadband light is generated in the Ti:sapphire oscillator, filtered in the acousto-optic element, guided by a multi-mode fiber where the modes are dynamically mixed and sent trough the Köhler illumination system onto the sample. Alternative brightfield illumination marked in green. The CMOS camera acquires the images and triggers the next optical frequency step.

#69358 - $15.00 USD Received 27 March 2006; revised 19 June 2006; accepted 20 June 2006

4. Methods

To compare 3D-teFD OCT with fast raster-scanning 1D-seFD and because of readily available camera technology the operational wavelength range was chosen to be set around 800 nm with a similar bandwidth for both systems. Thereby a broad bandwidth Titanium: sapphire laser, already tested for teTD [35] and seFD [22] imaging, in combination with a specially designed acousto-optic tunable element was used as a tunable light source for preliminary studies of the feasibility of time encoded frequency domain OCT. This oscillator emits a bandwidth at full width at half maximum of 110 nm centered at 790 nm. External spectral tuning could be performed over a little less than this bandwidth at an arbitrary number of optical frequency steps. Line width was less than 0.4 nm, due to the filtering characteristics of the acousto-optic element. Successive frequencies could be separated by ~13 µs without reducing the filter line width of the acousto-optic (AO) element. The high frequency driver was built upon a custom designed micro-controlled digital phase generator, capable of digitally synthesizing an arbitrary waveform up to 120 MHz. Local memory holds an arbitrary sequence of up to 4096 different frequencies with independent amplitude and holding time to allow for complete power and line width control during the scan, which not necessarily has to be executed in sequence. Frequency stepping, rather than the alternate mode of continuous tuning has the advantage of being able to select a specific, precisely defined optical frequency for every single scan, which solves the re-sampling problem found in common equidistant wavelength tuning and decouples filter line width from exposure time and scanning speed within the AO response time.

The light source emitted up to 1 mW (at the spectral peak) and was optically interfaced via a multimode fiber optic link to a commercially available infrared optical microscope (Axioskop 2 MAT, provided by Carl Zeiss Meditec, Austria) equipped with a 640 x 480 pixel CMOS (complementary metal oxide semiconductor) camera. The microscope head was modified by replacement of the standard beam splitter/filter unit with a 50:50 beam splitter based Michelson interferometer equipped with two identical microscope objectives (EPIPLAN 20x/0.5 or 5x/0.1 respectively) in the reference and sample arm, all optimized to support the whole illumination bandwidth. Due to the high sensitivity of Si-detectors at 800 nm only 50 µW at the entrance of the microscope were enough to get close to saturation of the detector array with a reflective target at 1 ms integration time, resulting in approximately 20 µW illumination power for the complete sample area. For low reflectance measurements the power in the reference arm had to be attenuated with a reflective neutral density filter to avoid saturation. Commonly 256-1024 two dimensional images, sampled at successive optical frequencies, were acquired in cycles of approximately 50 ms (depending on target reflectance and attenuation in the reference arm), which were only limited by the transfer time between the camera and the frame grabber.

Full-field approaches distribute the power transversally, while teFD additionally disperses optical power in time across different wavelengths. Hence the average power within one depth scan (=axial line like a single A-scan in scanning OCT) per frequency slot P_{Ascan} is 20 µW / (0.3 Mpx)= 66 pW/px in our case, which is 5-6 orders of magnitude lower than in scanning systems, therefore potentially allowing for much higher power on the sample, up to those found in standard light microscopy of around 100 mW. The average power has to be multiplied by the number of optical frequency steps n and the illumination time t_{il}. In this case: $n \cdot P_{Ascan} \cdot t_{il}$ = 1024·66 pW·50 ms = 3.4 nJ. Within a depth-scan the average energy deposited in one of the 512 volume elements (voxels) is 6.6 pJ. The reduction from 1024 frequencies to 512 axial planes is caused by the information loss due to the non-complex detection of the spatial frequencies in the Fourier transformation.

#69358 - $15.00 USD Received 27 March 2006; revised 19 June 2006; accepted 20 June 2006

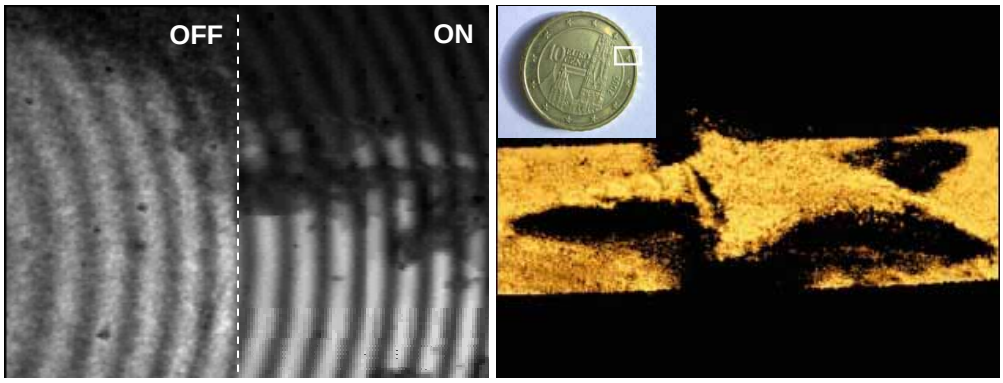

Fig. 3. left: acoustic mode mixer, reduction of typical speckle pattern on a partially reflective surface at single optical frequency illumination, in the movie (acousticMixerOnOff.avi, 3 MB) the sample is also moved as a whole; right: profilometry of a star on a 10 cent Euro-coin, rendering based on stack FD images (Ecoin-star.avi 1.5 MB)

5. Results

Utilizing Köhler illumination (Fig. 2) the fiber output is collimated; stray light is removed by an aperture and is focused onto the holographic diffuser for more uniform distribution of the Gaussian intensity profile. Further diaphragms limit the size of the illumination field and a lens focuses the beam to the inner focal plane of the objective. Therefore the zero delay of the object is placed in the Fourier-plane of the diffuser. A drawback in this narrow line width system with long axial coherence length is the strong transversal coherence in form of speckle like also found in holographic techniques [36] utilizing scanning sources. This kind of cross-talk by illumination with arbitrary phase from different points at the diffuser could be eliminated by mixing the high number of differently populated transversal modes in the multimode fiber by micro bending at acoustic frequencies, thus generating fast changing patterns of speckle. In the interferometer only conjugated points of the two arms interfere constructively during illumination time, while speckle from unassociated sites is averaged out during illumination time. Due to the Köhler illumination scheme the illumination beam is almost parallel, resulting in similar instantaneous patterns across the samples depth as well as in the reference arm. This also reduces cross-talk generated within a scattering sample. The reduction of speckle contrast on a plain target was measured with a mirror as sample, monitoring the variance of a bright region with activated and de-activated mode mixer. According to this measurement the gain in SNR was 12 dB. An example during interferometric measurement is shown in Fig. 3 left; the associated movie demonstrates temporal changes of the speckle pat-

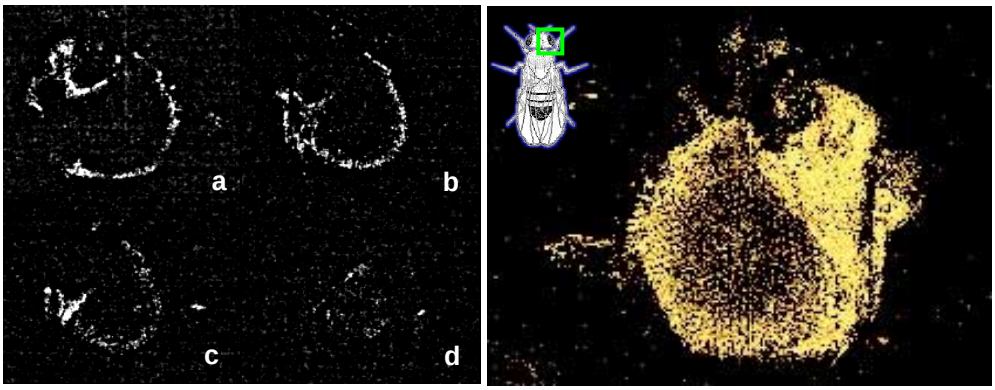

Fig. 4. Fruit fly (drosophila melanogaster) eye. Left: En face crosssections at successive depth. Right: the rendering unveils the volumetric nature of the eye, including the symmetric structure of single facets of the compound eye “Flyhead-Eye_3DteFD.avi” 1 MB

#69358 - $15.00 USD Received 27 March 2006; revised 19 June 2006; accepted 20 June 2006

tern when the mixer is deactivated. The dynamic range of the tomogram, describing the intensity ratio between noise intensity and averaged peak intensity of a reflective site close to saturation was found to be 36 dB. The commonly quoted signal to noise ratio (SNR) is measured by the maximum possible attenuation to detect a 100% reflective sample or the lowest reflectivity detectable in the sample. It is defined by the quotient between maximum signal intensity and average noise intensity and is mainly dependent on the illumination power and the acquisition time [18]. For the integrating CMOS used in this experiment the main limitation is set by the saturation power due to the static background of the signal. For low reflective samples the contribution of the reference arm prevails. Thereby a change in the splitting ratio in favor of the sample arm enhances the signal strength if the acquisition time is extended accordingly, but is also limited by detection noise of the camera. Even at these extremely low powers upon the sample the SNR can be elevated above 83 dB due to long overall integration time of 50 ms x 1024 = 50 s per A-scan. The theoretical SNR of this system can be derived from [18] by modifying the formula to account for the measurement at a specific volume element:

$$\mathbf{SNR} = \frac{\boldsymbol{\rho} \cdot \mathbf{P}_{\mathbf{vox}} \cdot \mathbf{R}_{\mathbf{vox}} \cdot \boldsymbol{\Delta}\mathbf{t}}{\mathbf{2} \cdot \mathbf{e}} \qquad (1)$$

Where the responsitivity ρ=0.1, P_{vox} = 15 µW/(640*480) is the power on the sample point and e~$1.6 \cdot 10^{-19}$ C is the electron charge. Assuming a reflectivity of $R_{vox} \sim 1$ for the silver mirror and a total acquisition time for 1024 different spectral slots of 50 ms per slot Δt = 51.2 s results in 89 dB. This indicates SNR loss in the system due to imperfect imaging conditions, e.g. overfilling of the sampling field with the illumination beam and reduced transmission in the optical components. Measurements using an USAF reflective resolution target revealed a transverse resolution of less than 4 µm as expected from the high NA objective. For investigation of scattering three dimensional structures ultrahigh resolution 3D teFD-OCT could be shown in similar resolution on a biological sample. Different portions of a fruit fly (drosophila melanogaster) were investigated; Fig. 4 left shows *en face* reconstructions of a portion of the fly's head, especially the eye-lobe. The rendering on the right side of Fig. 4 epicts the three-dimensional fine structure of planar facets of the compound eye; Fig. 5 left demonstrates a rendering of the three dimensional structure of the fly's hairy leg placed on top of a tilted glass plate (only drops of dried fluid used to fix the specimen are visible). On the right portion of Fig. 5 the same specimen was illuminated by the alternate halogen light in transmission geometry at 16 mW and with 1 ms shutter.

6. Discussion

Compared to a transversally scanning seFD-OCT system the 640 x 480 pixel scan in 50 s corresponds to ~6 klines/s. These systems nowadays approach a SNR of ~95 dB at >10 klines/s with about 1 mW of power [22], that equals an energy deposition of 100 nJ per depth-scan. In

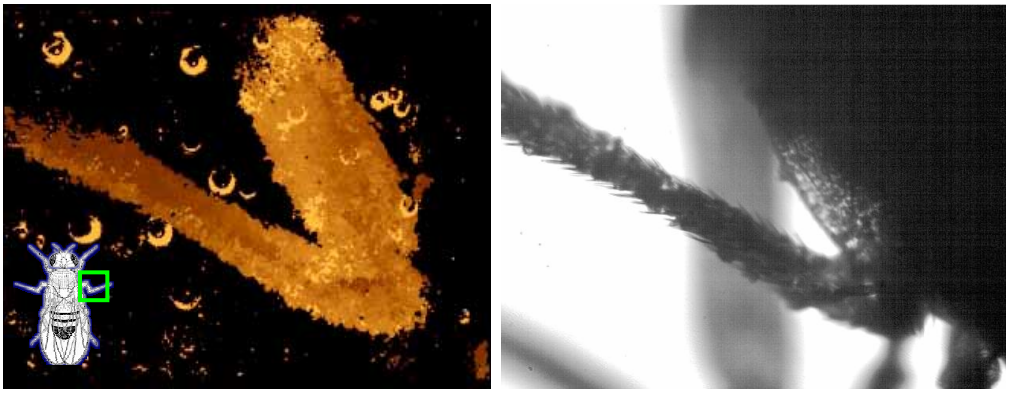

Fig. 5. left: Fruit-fly (drosophila melanogaster) leg, portion fixed to a tilted glass plate (not directly visible). Right: Transmission microscopy image of the identical specimen illuminated with white light.

#69358 - $15.00 USD Received 27 March 2006; revised 19 June 2006; accepted 20 June 2006

direct comparison this means that the 3D-teFD-OCT system, demonstrated in this paper actually performs only slightly worse (at similar energy deposition per pixel but elevated instantaneous power a SNR of 96 dB is expected). It also has potential to go for even much stronger illumination than applied in this work without getting close to similar instantaneous optical powers per area element.The SNR of the current teFD-OCT system is limited by the mechanic instabilities during the relatively long overall measurement time and the post processing, that currently ignores phase instability during the scan due to motion. This effect is often called "phase washout" and is also found in seFD-OCT, though currently due to lack of redundant measurements no means for suppression exist there, other than improving imaging speed.

The instabilities can be directly observed in the image when the images are acquired in the frequency domain and can be monitored in all three spatial directions. Mechanic shifts are identified when phase shifts appear in all pixels simultaneously, independent on the depth of the examined region. Tilts within groups of successive scans can be recognized as well. A compensation scheme was not integrated into the system, but is a viable option for future application. Post-processing in the presented tomograms was performed by simple restacking of the multiple images and one-dimensional pixel wise Fourier transformation as a function of optical frequency. Extraction of absolute values in the positive Time Domain (which halves the number of elements in depth, due to the non complex acquisition) resulted in 512 axial layers with depth spacing in the order of the coherence length, corresponding to ~3 µm in tissue in this case and approximately similar resolution in all three orthogonal directions. Arbitrary cross-sections were easily accessible by proper selection of a slice, as was full three dimensional rendering of the 160 Mvoxel volume. The availability of white light transillumination (halogen source) from below allowed for fast monitoring during alignment of the sample and direct comparison of the transmittance image with the 3D tomogram.

7. Conclusions

3D-teFD-OCT technology was proven to be a viable method for acquisition of ultrahigh resolution optical coherence tomograms. The image dynamics and SNR is already comparable to state of the art seFD-OCT technology at its native state. Future developments will have to include improvements of scanning speed with commercially available high-speed cameras together with higher power rapidly-tuned wavelength-swept light sources currently being developed and numeric phase correction to suppress artifacts and signal loss due to phase instabilities. In conclusion, it was demonstrated, for the first time, ultrahigh resolution, three dimensional time encoded frequency domain optical coherence tomography, enabling ultrahigh resolution imaging of sample volume information over 1.3 x 1 x 0.2 mm^3 by single tuning of the laser without the use of mechanical scanners neither for depth nor for transverse scanning nor in the laser itself. Employing state of the art technology in the future, this novel OCT technique promises to enable real time, high resolution three dimensional imaging at video rate.

Acknowledgments

We gratefully acknowledge support from Carl Zeiss Meditec , Andreas Stingl, Femtolasers Produktion GmbH, Austria, Daniel Kaplan from Fastlite, France. Contributions of T. Parheis, Technical University of Vienna, L. Schachinger, Medical University of Vienna are acknowledged as well. This work was financially supported in part by FWF P14218-PSY, FWF Y 159-PAT, CRAF-1999-70549 as well as the Christian Doppler Society, Femtolasers Produktion GmbH and School of Optometry, Cardiff University.

#69358 - $15.00 USD Received 27 March 2006; revised 19 June 2006; accepted 20 June 2006